

Post-thermal-quench shattered pellet injection for runaway electron seed depletion in ITER

E. Nardon, A. Matsuyama, D. Hu, F. Wieschollek

▶ **To cite this version:**

E. Nardon, A. Matsuyama, D. Hu, F. Wieschollek. Post-thermal-quench shattered pellet injection for runaway electron seed depletion in ITER. Nuclear Fusion, In press, 62, pp.026003. cea-03539301

HAL Id: cea-03539301

https://cea.hal.science/cea-03539301

Submitted on 21 Jan 2022

HAL is a multi-disciplinary open access archive for the deposit and dissemination of scientific research documents, whether they are published or not. The documents may come from teaching and research institutions in France or abroad, or from public or private research centers.

L'archive ouverte pluridisciplinaire **HAL**, est destinée au dépôt et à la diffusion de documents scientifiques de niveau recherche, publiés ou non, émanant des établissements d'enseignement et de recherche français ou étrangers, des laboratoires publics ou privés.

Post-thermal-quench shattered pellet injection for runaway electron seed depletion in ITER

E. Nardon[1], A. Matsuyama[2], D. Hu[3], F. Wieschollek[4]

[1]CEA, IRFM, F-13108 Saint-Paul-lez-Durance, France
[2]QST, Rokkasho Fusion Institute, Aomori 039-3212, Japan
[3]School of Physics, Beihang University, Beijing 100191, China
[4]Max Planck Institute for Plasma Physics, Boltzmannstr. 2, 85748 Garching b. M., Germany

E-mail: eric.nardon@cea.fr

Abstract. The possibility of using shattered pellet injection after the thermal quench of an ITER disruption in order to deplete Runaway Electron (RE) seeds before they can substantially avalanche is studied. Analytical and numerical estimates of the required injection rate for shards to be able to penetrate into the forming RE beam and stop REs are given. How much material could be assimilated before the Current Quench (CQ) becomes too short is also estimated. It appears that, if hydrogen pellets were used, the required number of pellets to be injected during the CQ would be prohibitive, at least considering the present design of the ITER Disruption Mitigation System (DMS). For neon or argon, the required number of pellets, although large, might be within reach of the ITER DMS, but the assimilated fraction would have to be very small in order not to shorten the CQ excessively. This study suggests that other injection schemes, based for example on small tungsten pellets coated with a low Z material, may be worth exploring as an option for an upgrade of the ITER DMS.

1. Introduction

Shattered Pellet Injection (SPI) is the reference concept for the ITER Disruption Mitigation System (DMS) [1][2]. One of the main objectives of the DMS is the avoidance of large Runaway Electron (RE) beams [3][4][5]. RE generation can be divided into primary and secondary generation. In ITER, since the Dreicer mechanism is expected to be negligible [5], there are essentially 3 primary (also called 'seed') RE generation mechanisms to consider. The first one, the hot tail mechanism, is difficult to predict. It could be very strong for a hot plasma with a fast Thermal Quench (TQ), as suggested by recent experimental findings [6]. On the other hand, it has been suggested that hot tail generation may be efficiently reduced by a fast plasma dilution before the TQ using pure deuterium (or hydrogen) SPI [7]. The other two seed generation mechanisms are the tritium β decay and the Compton scattering of γ rays emitted by the activated wall. These are very small but continuous RE seeds which will be present only during

the nuclear phase of ITER operation. The problem in large tokamaks such as ITER is that even very small RE seeds could give rise to large, multi-MA RE beams because of secondary RE generation by the avalanche effect [8]. The conclusion of a recent study with the GO code, in which it is considered that the plasma composition can be varied at will by injection of deuterium and neon/argon by the DMS, is indeed that during an ITER 15 MA DT plasma disruption, a multi-MA RE beam would be generated whatever the plasma composition, whenever the Current Quench (CQ) timescale is short enough from the point of view of electromagnetic loads [9].

The present paper discusses the following question: is it possible to deplete small RE seeds, in particular those from tritium decay and Compton scattering, before they have substantially avalanched, by injecting pellets, possibly shattered, counting on the stopping power of the shards/pellets (in the following, we will use only the term 'shards' for concision)? REs will typically travel across shards. Each time they will do so, they will lose a certain amount of energy. If this energy dissipation is fast enough compared to the acceleration by the loop voltage and the population growth from the avalanche, the formation of large RE beams might be avoided. But clearly, since RE seeds are continuously produced, a continuous injection or repeated discrete injections would be required.

The aim of this paper is to provide rough estimates to assess the feasibility of such a scheme. We will first discuss in Section 2 the 'degrees of freedom' in the design of the scheme, i.e. the different types of injections that can be envisaged. Then, we shall analyze the 3 main conditions which are required for the scheme to work. The first one is that shards should be able to stop RE seeds. This will be addressed analytically in Section 3 and numerically in Section 4. The second condition is that shards should be able to penetrate the forming RE beam, which will be discussed in Section 5. The third condition, addressed in Section 6, is that the material possibly assimilated by the plasma as a result of these injections should not make the CQ faster than tolerable. Finally, Section 7 will summarize results and discuss priorities for future work.

2. Degrees of freedom

Since RE seed production is a continuous process, the injection scheme should be based either on repeated injections or on a continuous injection, like shown schematically in Fig. 1. In this figure, the repeated injections (left plot) correspond to successive SPI from the Low Field Side (LFS) midplane, with a certain horizontal and vertical velocity spread of the shards. Such repeated injections are in principle possible with the present design of the ITER DMS. The continuous injection (right plot), on the other hand, is more conceptual and harder to approach with the present ITER DMS design. It consists in a steady beam of shards, also coming from the LFS, with all shards assumed to have the same, purely horizontal, velocity. Degrees of freedom common to both types of injection are the time-averaged solid mass flux and the averaged velocity of the shards. In the case of repeated injections, other degrees of freedom are the time delay between

injections and the shards velocity spread.

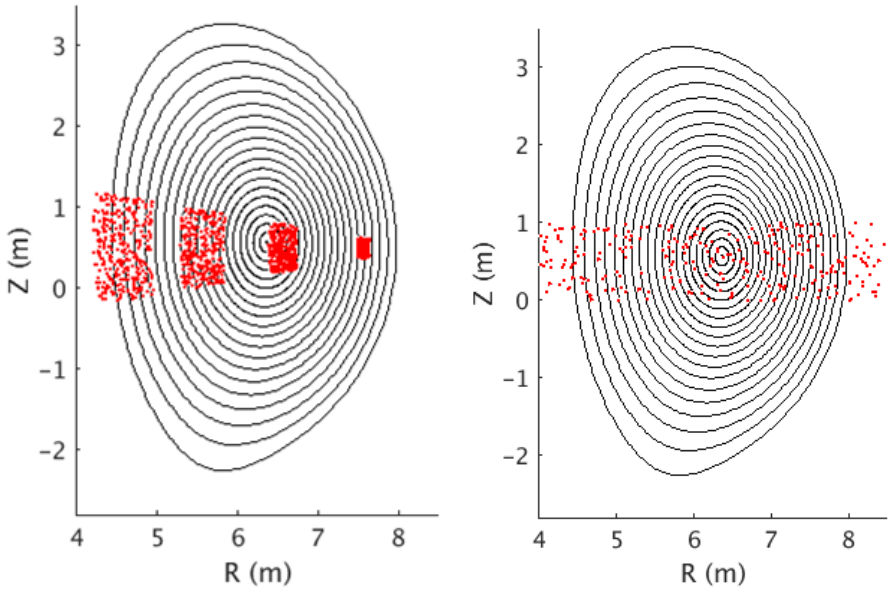


Figure 1. Schematic plots illustrating the concept of repeated (left) or continuous (right) injection(s).

Another important degree of freedom, as we shall see below, for both the repeated and continuous injection, is the size of the shards. Two limiting cases can be distinguished: the case of 'many small shards' and the case of 'a few large shards', as illustrated in Fig. 2. The key difference between these two cases is that in the former, there is at any instant a number of shards intercepting a given flux surface (during the passage of a shard cloud across that surface), while in the latter, there are temporal gaps between shards passages. Note that the 'few large shards' case should not necessarily be based on SPI but could also correspond to repeated injections of non-shattered pellets.

The last important degree of freedom is the pellet material. In this paper, we will consider pure hydrogen, neon or argon pellets since these are the species currently envisaged for the ITER DMS, but the results presented could easily be generalized to other species. The key trade-off is between stopping power and the risk to make the CQ too short, both being much smaller for hydrogen than for neon or argon, as we shall see below.

3. Can shards stop Runaway Electrons? Analytical estimates

Let us begin with analytical estimates to assess the possibility to stop REs with shards, assuming the latter penetrate into the forming RE beam. To simplify expressions, shards are assimilated to cubes of edge length $2r_s$, with the same r_s for all shards. A RE is typically energetic enough to travel across a shard. When it does so, it loses an energy $\Delta E = 2r_s p$, where p is the stopping power of the shard (assuming, for simplicity, that

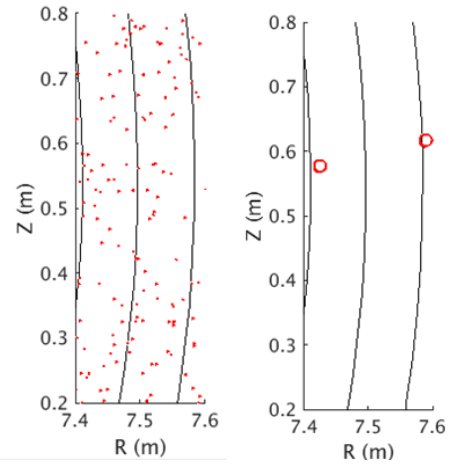


Figure 2. Schematic illustratiions of the 'many small shards' (left) and 'a few large shards' (right) cases.

the RE crosses the shard in a direction parallel to an edge). The averaged energy lost by a RE per toroidal turn in this process is:

$$E_{\mathrm{loss/turn}} = N_{\mathrm{shard/turn}} \Delta E \tag{1}$$

where $N_{\mathrm{shard/turn}}$ is the average number of shards encountered per turn. In order to estimate $N_{\mathrm{shard/turn}}$, in what follows we will assimilate RE drift surfaces to flux surfaces and assume that the poloidal position of a RE after a certain number of toroidal turns is equivalent to a random variable with a homogenous probability density over $[0, 2\pi]$ (this assumption will be justified in Section 4.4).

The energy gained by a RE from the loop voltage per toroidal turn is:

$$E_{\mathrm{gain/turn}} = eV_{\mathrm{loop}}. \tag{2}$$

We will use the value $V_{\mathrm{loop}} = 1.1$ kV, which is expected at the beginning of a CQ of exponential time constant 66 ms (corresponding to a duration of 150 ms in the 'usual' definition which consists in taking the exponential decay time between 80 and 20 % of the initial plasma current and dividing it by 0.6) for an initial poloidal flux of 75 V.s, which is a typical value for an ITER 15 MA plasma (this accounts for the presence of the highly conductive vacuum vessel) [10]. We chose here a CQ timescale in the upper range of what is considered tolerable [1], which is favorable for the discussed RE depletion scheme (on the other hand, we take V_{loop} at the beginning of the CQ, conservatively ignoring the fact that V_{loop} decays during the course of the CQ). It should be kept in mind that the results below are strongly sensitive to V_{loop} since $E_{\mathrm{gain/turn}}$ is directly proportional to it, considering that collisional drag should be negligible at relativistic energies (it should be equivalent to an electric field $E_c = 0.075 n_b c^2/v^2$ in V/m, where n_b is the background electron density in units of 10^{20} m^{-3}, c is the speed of light and v the electron velocity [4], to be compared to $V_{\mathrm{loop}}/2\pi R \simeq 30$ V/m for $V_{\mathrm{loop}} = 1.1$ kV) and that synchrotron radiation drag (which scales like the electron momentum squared at high energies, see

[3] and references therein) might become important only at energies of several MeV. A CQ timescale at the low end of what is considered tolerable in ITER, i.e. an exponential time constant of 22 ms [1], would increase V_{loop} by a factor 3 and severely impact the required quantities for the proposed scheme.

A first condition for a successful depletion of the RE seed population is:

$$\frac{E_{\mathrm{gain/turn}}}{E_{\mathrm{loss/turn}}} < 1. \tag{3}$$

This condition is sufficient to fully stop REs in the case of a continuous injection of many small shards. On the other hand, for repeated injections separated by gaps or for the case of a few large shards, REs may re-accelerate during the time intervals when no shards are passing (the acceleration time of an electron from rest up to 10 MeV, neglecting any drag, is $\simeq 1$ ms in ITER with $V_{\mathrm{loop}} = 1.1$ kV). In these cases, another necessary condition for success is thus:

$$\frac{t_{\mathrm{stop}}}{t_{\mathrm{pass}}} < 1 \tag{4}$$

where t_{stop} is the time it takes to stop a RE and t_{pass} is the time during which the shard cloud (in the case of repeated injections with many small shards) or an individual shard (in the case of a few large shards) passes across the surface where the RE is located.

We shall now provide estimates for $E_{\mathrm{gain/turn}}/E_{\mathrm{loss/turn}}$ and $t_{\mathrm{stop}}/t_{\mathrm{pass}}$ for the case of many small shards in Section 3.1 and for the case of a few large shards in Section 3.2.

3.1. Case of many small shards

In the case of many small shards, the number of shards which intersect a given flux surface is $N_{s@\psi} \simeq 2r_s dN_s/dr_\psi$, where dN_s/dr_ψ is the shard number density with respect to the minor radial coordinate r_ψ, and the $2r_s$ factor is an estimate of the extension of shards along the minor radius.

The fraction of the poloidal perimeter of the flux surface which is intercepted by a given shard is $f_\theta \simeq 2r_s/(2\pi r_\psi)$, assuming flux surfaces have a circular cross-section. It can be remarked that, due to the $1/r_\psi$ factor, shards will brake REs more easily in the core than at the edge. The average number of shards that a RE encounters per toroidal turn is then:

$$N_{\mathrm{shard/turn}} = N_{s@\psi} f_\theta \simeq \frac{2r_s^2}{\pi r_\psi}\frac{dN_s}{dr_\psi}, \tag{5}$$

resulting in an average energy loss per turn:

$$E_{\mathrm{loss/turn}} \simeq \frac{4r_s^3 p}{\pi r_\psi}\frac{dN_s}{dr_\psi} \tag{6}$$

It thus appears that $E_{\mathrm{loss/turn}} \propto d(N_s r_s^3)/dr_\psi \propto d(N_s V_s)/dr_\psi$, where V_s is the shard volume. In other terms, $E_{\mathrm{loss/turn}}$ is proportional to the radial derivative of the total

volume occupied by the shard population. This can be understood when considering the problem from the point of view of shards instead of electrons. Indeed, shards are permanently being travelled across by a RE flux of density $cn_{\rm RE}$ (note that here we assume, for simplicity, relativistic REs travelling at the speed of light) and $n_{\rm RE}$ is the RE density (assumed homogeneous). This corresponds to a power dissipation in each shard equal to $cn_{\rm RE}pV_s$. The radial derivative of the power dissipated in shards is thus $cn_{\rm RE}pV_s dN_s/dr_\psi$. The power lost by each RE is approximately $E_{\rm loss/turn}c/(2\pi R)$, where R is the major radius. Thus the radial derivative of the power lost by all REs is $E_{\rm loss/turn}c/(2\pi R)dN_{\rm RE}/dr_\psi$, with $dN_{\rm RE}/dr_\psi = n_{\rm RE} \times 2\pi r_\psi \times 2\pi R$. Equating the two preceding expressions for the radial derivative of the power dissipated in shards, one finds:

$$E_{\rm loss/turn} \simeq \frac{V_s p}{2\pi r_\psi}\frac{dN_s}{dr_\psi}. \tag{7}$$

Considering that, to obtain Eq. 6, we had assimilated shards to cubes of edge length $2r_s$ and thus of volume $8r_s^3$, Eqs. 6 and 7 are consistent with each other. However, Eq. 7 is more general.

An important comment here is that $E_{\rm loss/turn}$ does not depend on the shard radius r_s, i.e. the shard size distribution does not affect $E_{\rm loss/turn}$ (as long as the 'many small shards' regime is valid).

Let us make first numerical estimations. Concerning the stopping power p, we shall conservatively use the minimal value with respect to the electron energy, which is reached near 1 MeV. This should suffice for the rough estimates we are aiming at here, since p varies moderately (i.e. by 50% or less) with the electron energy in the range 1-10 MeV. The minimal ESTAR stopping power is 3.8 MeV.cm^2/g for hydrogen, 1.6 MeV.cm^2/g for neon and 1.4 MeV.cm^2/g for argon [11] which, multiplied by the respective solid density of these materials, gives 38 MeV/m for hydrogen and 230 MeV/m for both neon and argon. Condition 3 thus corresponds to $V_s dN_s/dr_\psi > 5.3 V_{\rm 28mm}$/m for hydrogen and $V_s dN_s/dr_\psi > 0.87 V_{\rm 28mm}$/m for neon or argon, where $V_{\rm 28mm}$ is the volume of a large ITER DMS pellet under the present design, i.e. of a cylinder of diameter 28 mm and length 56 mm ($V_{\rm 28mm} = 3.4 \times 10^{-5}$ m^3). We will refer to these pellets as '28 mm pellets' in the following. This means that the volume of shard material should correspond to more than 5.3 (resp. 0.87) 28 mm pellets per meter for hydrogen (resp. neon or argon).

We shall now specialize the above expression for $E_{\rm loss/turn}$ to the case of a shard cloud from a single SPI. In this case, $dN_s/dr_\psi = N_s/L_{\rm cloud}$, where N_s is the number of shards in the cloud and $L_{\rm cloud}$ is the radial extension of the cloud. The latter is related to the velocity spread of the shards Δv_s in the following way: $L_{\rm cloud} = l\Delta v_s/\langle v_s\rangle$, where $\langle v_s\rangle$ is the average shard velocity and $l = r_{s0} - r_\psi$ is the distance shards need to travel to reach the flux surface under consideration from their initial position $r = r_{s0}$. Thus:

$$E_{\rm loss/turn} \simeq \frac{V_s p N_s \langle v_s\rangle}{2\pi r_\psi (r_{s0} - r_\psi)\Delta v_s}. \tag{8}$$

In the present ITER DMS design, $r_{s0} \simeq a + 0.35$ m, where $a \simeq 2$ m is the plasma minor radius [12]. Fig. 3 shows $E_{\rm gain/turn}/E_{\rm loss/turn}$ as a function of r_ψ, for $\Delta v_s/\langle v_s\rangle = 0.2$

and for a hydrogen, neon or argon 28 mm pellet. It can be seen that a single hydrogen pellet is not sufficient to brake REs everywhere in the plasma, although it is sufficient in the very core and very edge, but two synchronized pellets should be sufficient. On the other hand, a single neon or argon pellet should easily be able to brake REs throughout the plasma, and one fourth of a pellet should be marginally sufficient.

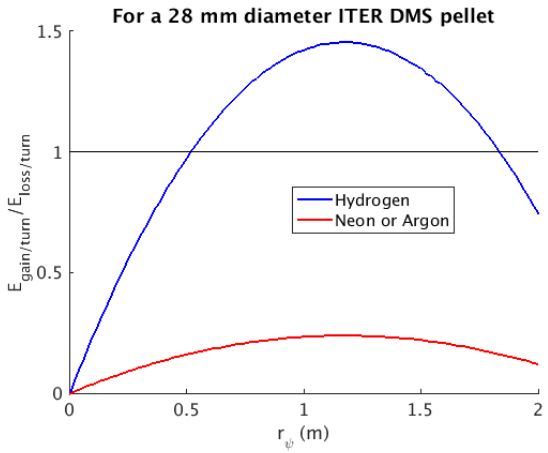


Figure 3. $E_{gain/turn}/E_{loss/turn}$ ratio as a function of the flux surface minor radius r_ψ, for $\Delta v_s/\langle v_s\rangle = 0.2$ and for a 28 mm hydrogen, neon or argon pellet shattered into many small shards, taking the minimal (with respect to the electron energy) ESTAR stopping power and considering that $V_{loop} = 1100$ V.

As discussed above, for the case of repeated SPI with gaps between shard clouds, we should also estimate $t_{\rm stop}/t_{\rm pass}$. The stopping time, assuming that the RE travels across many shards during the passage of the shard cloud, is:

$$t_{\rm stop} \simeq \frac{2\pi R}{c}\frac{E_{\rm RE}}{E_{\rm loss/turn} - E_{\rm gain/turn}} \tag{9}$$

where $E_{\rm RE}$ is the initial kinetic energy of the RE. The time it takes for the shard cloud to pass across a flux surface is:

$$t_{\rm pass} = \frac{L_{\rm cloud}}{\langle v_s\rangle} = (r_{s0} - r_\psi)\frac{\Delta v_s}{\langle v_s\rangle^2}. \tag{10}$$

We thus have:

$$\frac{t_{\rm stop}}{t_{\rm pass}} = \frac{2\pi R}{c}\frac{E_{\rm RE}}{E_{\rm loss/turn} - E_{\rm gain/turn}}\frac{1}{r_{s0} - r_\psi}\frac{\langle v_s\rangle^2}{\Delta v_s}. \tag{11}$$

In the limit $E_{\rm loss/turn} \gg E_{\rm gain/turn}$, this simplifies to:

$$\frac{t_{\rm stop}}{t_{\rm pass}} \simeq \frac{4\pi^2 R r_\psi E_{\rm RE}\langle v_s\rangle}{c N_s V_s p}. \tag{12}$$

Not suprisingly, $t_{\rm stop}/t_{\rm pass}$ is proportional to $\langle v_s\rangle$, meaning that slower shards are beneficial for stopping REs. On the other hand, $t_{\rm stop}/t_{\rm pass}$ is independent of Δv_s. This is because both $t_{\rm stop}$ and $t_{\rm pass}$ are proportional to $1/\Delta v_s$: a cloud with less velocity spread

is more 'packed together' and thus brakes REs faster due to its larger shard density, but it also passes faster across the surface, and the two effects compensate each other.

Fig. 4 shows $t_{\rm stop}/t_{\rm pass}$ for $E_{\rm RE} = 10$ MeV as a function of $\langle v_s \rangle$ at $r_\psi = 1$ m (i.e. mid-radius) (left) and as a function of r_ψ for $\langle v_s \rangle = 100$ m/s (right) for a single 28 mm hydrogen, neon or argon pellet. It appears that a neon or argon pellet easily fulfills $t_{\rm stop}/t_{\rm pass} < 1$, while a hydrogen pellet needs to be slow enough and may be efficient only in the core region (furthermore, the assumption $E_{\rm loss/turn} \gg E_{\rm gain/turn}$ does not hold for such a pellet as we have seen above, so Fig. 4 is over-optimistic).

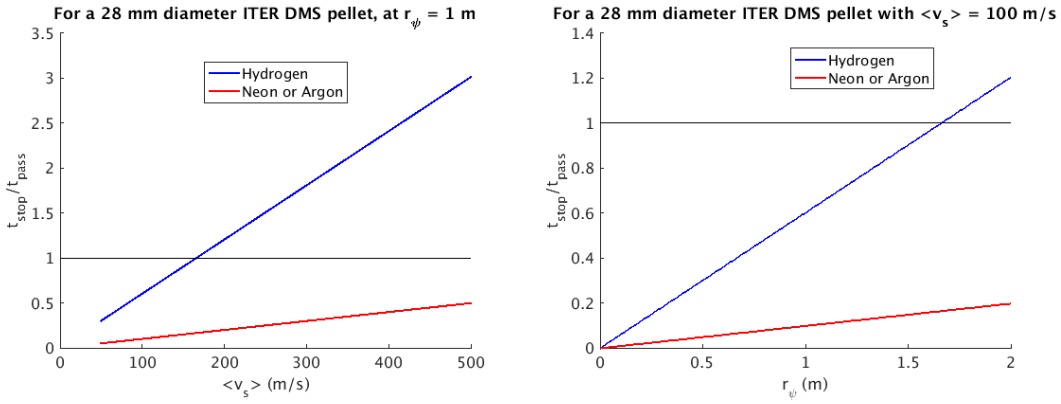


Figure 4. $t_{\rm stop}/t_{\rm pass}$ (in the limit where $E_{\rm loss/turn} \gg E_{\rm gain/turn}$) for $E_{\rm RE} = 10$ MeV as a function of $\langle v_s \rangle$ at $r_\psi = 1$ m (i.e. mid-radius) (left) and as a function of r_ψ for $\langle v_s \rangle = 100$ m/s (right) for a single 28 mm hydrogen, neon or argon ITER DMS pellet shattered into many small shards. The black horizontal line indicates $t_{stop}/t_{pass} = 1$, i.e. the limit above which REs are not fully stopped.

Note that Eq. 9 assumes that the RE travels at the speed of light, which is not accurate for weakly relativistic REs, for which c should in principle be replaced by the RE velocity $v_{\rm RE}$ in Eq. 9. It can however be noted that the ratio $E_{\rm RE}/v_{\rm RE}$ increases with the RE energy. Therefore, the stopping time of weakly relativistic REs is necessarily smaller than that of highly relativistic REs, for which Eq. 9 is appropriate. It is thus conservative to estimate $t_{\rm stop}$ through Eq. 9 for highly relativistic REs. In Fig. 4, we have assumed $E_{\rm RE} = 10$ MeV. This is at the high end of the energy spectrum of the Compton scattering source, while tritium β decay produces much less energetic electrons (< 18 keV) [5]. The above estimates should thus conservatively cover all seed REs from Compton scattering or tritium β decay. It is also plausible that energy-limiting processes such as synchrotron radiation will prevent the RE energy from getting much larger than 10 MeV.

An important point, however, is that the above considerations are valid only if the RE has time to travel across many shards during the passage of the shard cloud, which is a key assumption of Eq. 9. It is essential to assess whether this is the case. The typical time needed for a RE to hit a shard is:

$$t_{\rm hit} = \frac{2\pi R}{v_{\rm RE} N_{\rm shard/turn}} \simeq \frac{\pi^2 R r_\psi}{v_{\rm RE} r_s^2 dN_s/dr_\psi}, \tag{13}$$

where we have inserted Eq. 5 to obtain the second equality. Now, inserting $dN_s/dr_\psi = N_s/L_{\rm cloud} = N_s/(\langle v_s\rangle t_{\rm pass})$, we get:

$$\frac{t_{\rm hit}}{t_{\rm pass}} \simeq \frac{\pi^2 R r_\psi \langle v_s\rangle}{v_{\rm RE} r_s^2 N_s}. \tag{14}$$

It can be noticed that, in contrast with $t_{\rm stop}/t_{\rm pass}$, the ratio $t_{\rm hit}/t_{\rm pass}$ depends on the shard radius r_s. Since $N_s \propto r_s^{-3}$, we see that $t_{\rm hit}/t_{\rm pass} \propto r_s$, which is logical: a smaller shard radius implies a larger poloidal coverage by the shards and thus more frequent interactions between REs and shards (but with a smaller energy loss per interaction). As a lower bound for $v_{\rm RE}$, we take the critical velocity needed to run away. This velocity may be estimated to [4] $v_{\rm RE}^c \simeq (0.075 n_b \frac{2\pi R}{V_{\rm loop}})^{0.5} c$, where n_b is the background electron density in units of 10^{20} m^{-3}. Assuming $n_b = 1$, a typical value for ITER (conservatively not accounting for a possible density rise resulting from a massive material injection), gives $v_{\rm RE}^c \simeq 1.5 \times 10^7$ m/s. Considering a 28 mm pellet with $\langle v_s\rangle = 100$ m/s, $r_s = 1$ mm and $r_\psi = 1$ m, one finds $t_{\rm hit}/t_{\rm pass} \simeq 0.09$, i.e. about 11 interactions with shards during the passage of the shard cloud, validating the assumption made in Eq. 9 for these parameters.

3.2. Case of a few large shards

Let us now consider the case of a few large shards. As in the previous section, we shall begin by assimilating shards to cubes of side length $2r_s$ for simplicity. When a shard intersects a given flux surface, it occupies a fraction $\simeq 2r_s/(2\pi r_\psi)$ of its poloidal perimeter, which corresponds to the probability that a RE located on that surface passes through the shard per toroidal turn. When multiplied by $\Delta E = 2r_s p$, this results in:

$$E_{\rm loss/turn} \simeq \frac{4r_s^2 p}{2\pi r_\psi}. \tag{15}$$

If we now consider the more realistic case of spherical shards, the averaged value of $E_{\rm loss/turn}$ over the passage of the shard across the flux surface can be calculated by integrating over the shard passage:

$$E_{\rm loss/turn} \simeq \int_{x=0}^{2r_s} \frac{4(r_s^2 - x^2)p}{2\pi r_\psi}\frac{dx}{2r_s} = \frac{V_s p}{2\pi r_\psi}\frac{2}{\pi r_s}, \tag{16}$$

providing a more general expression for $E_{\rm loss/turn}$ which is consistent with Eq. 15. Eq. 16 is also consistent with the expression obtained for the case of many small shards, Eq. 7, replacing dN_s/dr_ψ by $2/(\pi r_s)$.

The condition $E_{\rm gain/turn}/E_{\rm loss/turn} < 1$ can then be written:

$$r_s > \sqrt{\frac{3\pi r_\psi e V_{\rm loop}}{4p}}, \tag{17}$$

which translates to $r_s > 8.3$ mm for hydrogen and $r_s > 3.4$ mm for neon or argon, for $r_\psi = 1$ m.

The time it takes for a spherical shard to pass across a flux surface is $t_{\rm pass} = 2r_s/v_s$, where v_s is the shard radial velocity. We thus have, making use of Eq. 16 and assuming again $E_{\rm loss/turn} \gg E_{\rm gain/turn}$ and considering highly relativistic REs (which can be justified by the fact that $E_{\rm RE}/v_{\rm RE}$ increases with the RE energy, as argued in the previous section):

$$\frac{t_{\rm stop}}{t_{\rm pass}} \simeq \frac{\pi^3 R E_{\rm RE} r_\psi v_s}{c V_s p}, \tag{18}$$

which translates to $r_s > 16$ mm for hydrogen and $r_s > 8.6$ mm for neon or argon, assuming $v_s = 100$ m/s. These shard radii are roughly twice larger than those found from the condition $E_{\rm gain/turn}/E_{\rm loss/turn} < 1$, thus justifying *a posteriori* the assumption $E_{\rm loss/turn} \gg E_{\rm gain/turn}$ (note that $E_{\rm loss/turn} \propto r_s^2$). It therefore appears that in the 'few large shards' regime, shards indeed need to be quite large. Assuming that shards result from the shattering of a 28 mm pellet, the requirement $r_s > 16$ mm (resp. $r_s > 8.6$ mm) corresponds to no more than $\simeq 2$ (resp. $\simeq 13$) shards per pellet, which appears difficult, if not impossible. Repeated injections of smaller non-shattered pellets may be better suited for this purpose.

As for the case of many small shards (previous section), it is essential to note that the above estimates assume a large number of interactions with the shard during its passage across the flux surface, i.e. $t_{\rm hit}/t_{\rm pass} \ll 1$, and this assumption should be assessed. In the present context, we have:

$$\frac{t_{\rm hit}}{t_{\rm pass}} \simeq \frac{\pi^2 R r_\psi v_s}{v_{\rm RE} r_s^2}. \tag{19}$$

If we consider again $v_{\rm RE} = v_{\rm RE}^c \simeq 1.5 \times 10^7$ m/s, $v_s = 100$ m/s, $r_\psi = 1$ m, we find $t_{\rm hit}/t_{\rm pass} \simeq 4 \times 10^{-4}/r_s^2$, implying that r_s needs to be substantially larger than 2 cm for the ratio $t_{\rm hit}/t_{\rm pass}$ to be small. This is larger than the radius found from Eq. 18, and thus appears more restrictive. However, our estimate for $t_{\rm hit}$ is too conservative for the vast majority of REs. Indeed, due to the $\propto 1/v_{\rm RE}^2$ decay of the collisional drag force, and unless $v_{\rm RE}$ is initially very close to $v_{\rm RE}^c$, a RE which does not run into the shard will reach velocities much larger than $v_{\rm RE}^c$ in a time shorter than $t_{\rm pass}$. For example, a RE with an initial parallel velocity $v_{\rm RE} = 1.0001 v_{\rm RE}^c$ submitted to an acceleration by the parallel electric field and a collisional drag from the background electrons reaches $\simeq c/2$ in 5×10^{-5} s, which is much smaller than $t_{\rm pass} \simeq 2 \times 10^{-4}$ s for $r_s = 1$ cm and $v_s = 100$ m/s. If we replace $v_{\rm RE}$ by $c/2$ in Eq. 19, we obtain $t_{\rm hit}/t_{\rm pass} \simeq 4 \times 10^{-5}/r_s^2$, and now it appears that r_s only needs to be substantially larger than 6 mm for the ratio $t_{\rm hit}/t_{\rm pass}$ to be small. For the parameters considered here, the condition $t_{\rm hit}/t_{\rm pass} \ll 1$ therefore does not appear to be more restrictive than the condition $t_{\rm stop}/t_{\rm pass} \ll 1$.

4. Can shards stop Runaway Electrons? Numerical simulations

The above estimates are useful as a first approach to the problem, but they are based on several simplifying assumptions. As a second step in our study, we will now introduce more realistic, although still largely simplified, numerical simulations.

4.1. Model description

For simplicity, REs are assumed to follow field lines. All shards are considered to be spheres with the same radius r_s, which remains constant in time. The model evolves by discrete steps, each step corresponding to one toroidal turn made by the REs. At each step, time is incremented by $2\pi R/v_{\mathrm{RE}}$, where v_{RE} is the RE velocity from the previous step (each RE has its own time), and the poloidal angle of the electron is incremented by $2\pi/q$, where q is the safety factor. Then, the position $(R_{\mathrm{RE}}, Z_{\mathrm{RE}})$ of the RE in Cartesian coordinates is calculated and the RE energy is incremented by:

$$\Delta E_{\mathrm{RE}} = eV_{\mathrm{loop}} - p\sum_{i_s=1}^{N_s} d_i \tag{20}$$

where $d_i \equiv 2\sqrt{\max(r_s^2 - (R_{\mathrm{RE}} - R_s(i_s,t))^2 - (Z_{\mathrm{RE}} - Z_s(i_s,t))^2, 0)}$ is the distance travelled across each shard, with $(R_s(i_s,t), Z_s(i_s,t))$ the position of shard i_s at time t. However, the RE energy is not allowed to get larger than 10 MeV, which is a simplified way to account for energy-limiting processes such as synchrotron radiation. The new RE velocity is then calculated from its updated energy by $v_{\mathrm{RE}} = c \times \sqrt{1 - 1/\gamma^2}$, with $\gamma = E_{\mathrm{RE}}/(m_e c^2)$, m_e being the electron rest mass.

We consider two types of magnetic geometries. The first one has flux surfaces of circular cross-section with the poloidal angle in straight field line coordinates θ^* taken to be the geometrical angle (the toroidal angle also being the geometrical one). The second geometry is from a realistic JET equilibrium scaled up to the size of ITER. Fig. 5 shows these 2 geometries.

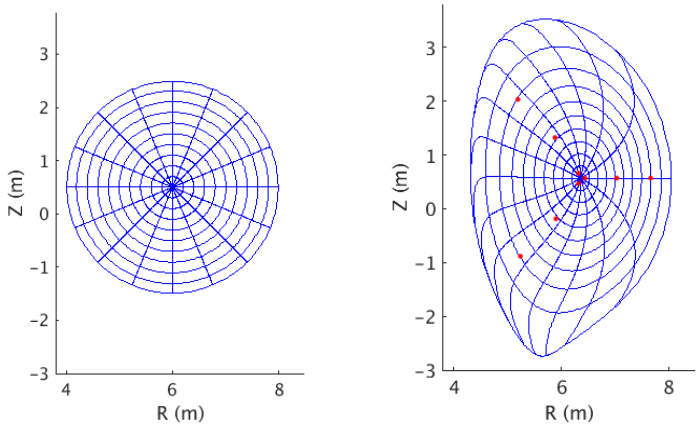


Figure 5. Geometry of the circular (left) and realistic (right) equilibria used for numerical simulations. Lines show iso-contours of the poloidal flux and of the straight field line poloidal angle (taking the geometric angle as the toroidal angle). In the right figure, red dots indicate the starting positions of the REs in the simulations described in Section 4.3.

4.2. Testing analytical predictions

Fig. 6 shows the minimal energy reached by a RE located on the $r_\psi = 1$ m surface over the passage of either a cloud of 1000 shards resulting from the shattering of a 28 mm pellet, representative of the 'many small shards' case (left), or a single shard of radius 1 cm, representative of the 'few large shards' case (right), as a function of the (mean) shard velocity, and for the circular (blue) and realistic (red) equilibrium geometries. The material is neon or argon in both cases. Vertical lines indicate the threshold velocity above which REs would not be stopped according to our analytical estimates, see Eq. 12 and 18. It can be seen that the analytical estimate works quite well for the circular geometry, for both 'many small shards' and 'a few large shards', but overpredicts the critical velocity for the realistic geometry. This is partly a consequence of the fact that in our analytical estimate, we have under-estimated the poloidal perimeter of the flux surface by using $2\pi r_\psi$. In addition, it can be guessed from iso-θ^* lines in Fig. 5 (right) that the θ^* of a field line after a random number of toroidal turns does not have a homogeneous probability density over $[0, 2\pi]$, and in particular has a smaller probability density near $\theta^* = 0$ (where shards are located), especially for flux surfaces in the outer part of the plasma. These two effects tend to reduce $E_{\mathrm{loss/turn}}$ and thus increase $t_{\mathrm{stop}}/t_{\mathrm{pass}}$, qualitatively explaining observations. It can be noted in Fig. 6 that the minimal energy reached by the RE as a function of the (mean) shard velocity presents large fluctuations. These are of statistical nature and are related to the relatively modest number of interactions with shards.

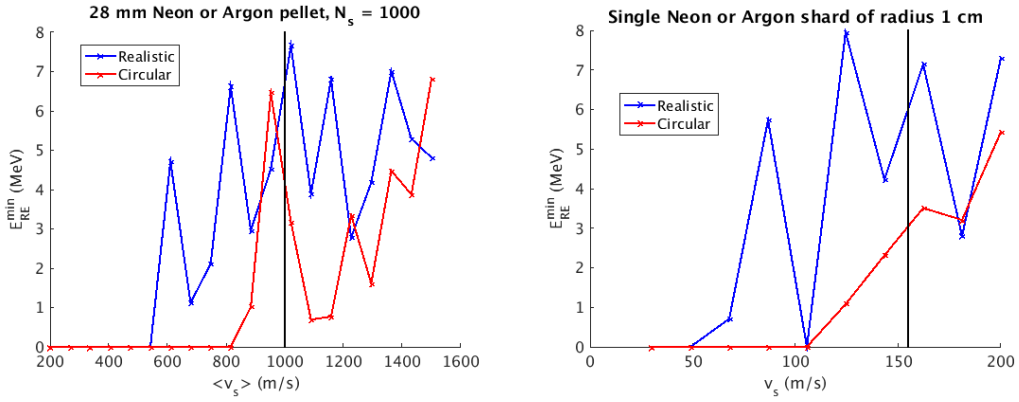


Figure 6. Minimal energy reached by a RE located on the $r_\psi = 1$ m surface over the passage of either a cloud of 1000 shards resulting from the shattering of a 28 mm pellet (left) or a single shard of radius 1 cm (right), as a function of the (mean) shard velocity. The material is neon or argon in both cases. The vertical lines indicate the critical (mean) shard velocity for stopping REs according to Eq. 12 (left) and 18 (right).

4.3. Injection parameters allowing to stop Runaway Electrons

In order to seek injection parameters allowing to stop REs, we use simulations in realistic geometry with REs initialized at 3 radial positions equally spaced between $\sqrt{\psi_n} = 0.05$

	H	Ne	Ar	Unit
Many small shards, continuous	6	0.9	0.9	# of 28 mm pellets/m
Many small shards, repeated	5	0.9	0.9	# of 28 mm pellets/injection
Single shard, repeated	1.5	0.3	0.3	Shard volume converted into # of 28 mm pellets

Table 1. Required injection rate to stop REs for a(n) (averaged) shard velocity of 100 m/s (see text for details)

and $\sqrt{\psi_n} = 0.8$, where $\psi_n \equiv (\psi - \psi_{axis})/(\psi_{bnd} - \psi_{axis})$ is the normalized poloidal magnetic flux (ψ_{axis} and ψ_{bnd} being the poloidal flux on the magnetic axis and at the last closed flux surface) and at 3 poloidal positions equally spaced in θ^* between 0 and 2π. The initial positions of the REs are indicated by red dots in Fig. 5 (right). We do not consider REs beyond $\sqrt{\psi_n} = 0.8$ because as one approaches the LCFS, REs become more and more difficult to stop, probably (mainly) because of the above-mentioned θ^* effect. RE formation might be avoided in the edge region by applying resonant magnetic perturbations [14].

For the case of many small shards and a continuous injection, we consider a shard size corresponding to a 28 mm pellet shattered into 1000 shards. We find that the threshold in terms of solid material volume per unit length (recall the discussion below Eq. 6) to stop REs is equivalent to about 6 (resp. 0.9) 28 mm pellets/meter for hydrogen (resp. neon or argon). These values are close to analytical esimates from Section 3.1, which may seem surprising since we have seen above that analytical estimates tend to be over-optimistic. This is explained by the fact that in the simulation considered here, the beam of shards extends across the whole plasma, meaning that it intersects each flux surface twice, whereas the analytical estimate takes into account a single intersection.

For the case of many small shards and repeated discrete injections, we consider the simultaneous injection of a certain number of 28 mm pellets, each shattered into 1000 shards, with an averaged shard velocity $\langle v_s \rangle = 100$ m/s and a relative shard velocity spread $\Delta v_s / \langle v_s \rangle = 0.2$. We find that the threshold number of pellets to stop REs is about 5 (resp. 0.9) for hydrogen (resp. neon or argon).

For the case of a few large shards, we consider a single shard launched from the LFS midplane and travelling across the plasma at $v_s = 100$ m/s. We find that the threshold shard radius for stopping REs is about 2.3 cm (resp. 1.4 cm) for hydrogen (resp. neon or argon), which corresponds to about 1.5 (resp. 0.9) times the volume of a 28 mm pellet.

The injection rates required to stop REs found in the different cases above are summarized in Table 1.

4.4. Effect of rational surfaces

It may be expected that some REs located on low order rational surfaces will remain outside the region where shards pass. While this is clearly true exactly on a rational surface, a more important question is up to what distance from the rational surface this

remains true. To address this question, Fig. 7 shows the minimal energy reached by REs during the passage of the shard cloud, as a function of the RE radial position, for a case with 3 large hydrogen pellets with $\langle v_s \rangle = 200$ m/s. REs are initialized away from the region where the cloud passes. The vertical line indicates the position of the $q = 2$ surface. It can be seen that indeed, REs initialized around $q = 2$ are not braked at all, but this is true only up to a radial distance smaller than 10^{-4} of the minor radius. This is because magnetic shear, combined with the fast velocity of REs, causes a strong precession in θ^* of the REs in a given poloidal plane over the duration of the cloud passage. With an axisymmetric magnetic field, rational surfaces therefore do not seem to pose a major threat to the proposed scheme. On the other hand, the existence of magnetic islands in the plasma could pose a problem since the helical transform is constant inside the islands. This question is left for future work.

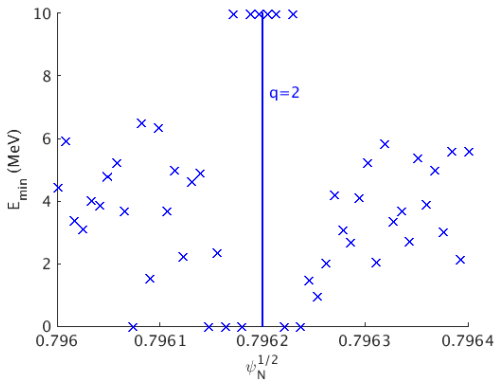


Figure 7. Minimal energy reached by REs during the passage of the shard cloud, as a function of the RE radial position. The vertical line indicates the position of the $q = 2$ surface.

5. Can shards penetrate into the Runaway Electron beam?

As is well known from present experiments, a large RE population is capable of vaporizing solid pellets very efficiently. The considered scheme can work only if the RE population always remains sufficiently small that shards can easily travel across the RE beam without being vaporized (on the other hand, we assume that melting would not be an issue). The energy deposited by REs into a given shard during its travel across the plasma is, per unit volume:

$$\mathcal{E}_{\rm heat} \simeq \frac{2 G_{\rm av} j_{\rm RE}^{\rm seed} p a}{e v_s} \tag{21}$$

where $j_{\rm RE}^{\rm seed}$ is the RE seed current density and $G_{\rm av}$ is the avalanche gain. The 'no vaporization' condition can be written $\mathcal{E}_{\rm heat} \ll \mathcal{E}_{\rm vap}$, where $\mathcal{E}_{\rm vap}$ is the shard vaporization heat per unit volume, which can be converted into a condition on $G_{\rm av}$. Since $G_{\rm av} = \exp(\Delta t / t_{\rm e-fold})$ with $t_{\rm e-fold}$ the avalanche e-fold time and Δt the time

	H	Ne	Ar
Many small shards, repeated	1000	180	180
Single shard, repeated	300	60	60

Table 2. Required injection rate for shards to be able to penetrate, in equivalent number of 28 mm pellets/s (see text for details).

during which the avalanche is free to develop, which in the present case is the temporal gap between (clouds of) shards, one can deduce a condition on Δt.

In ITER, the RE seed current from tritium β decay and Compton scattering is expected to be in the Ampère range [10], such that $j_{\mathrm{RE}}^{\mathrm{seed}} \sim 0.1$ A/m^2. Considering that the poloidal flux variation corresponding to an avalanche e-fold is $\simeq 2.3$ V.s [10] and that $V_{\mathrm{loop}} = 1.1$ kV, we have $t_{\mathrm{e-fold}} \simeq 2.1$ ms. Introducing the value of $\mathcal{E}_{\mathrm{vap}}$, which is $\simeq 19$, 120 and 260 MJ/m^3 for hydrogen, neon and argon respectively, we estimate that the Δt corresponding to vaporization is about 10 ms for all three materials. If we require for example a margin to vaporization (in terms of deposited energy) by a factor 10, the maximum allowable temporal gap between (clouds of) shards is about 5 ms, corresponding to an injection frequency of 200 Hz. If we multiply the quantities per injection required to stop REs given in Table 1 by this frequency, we obtain the injection rates given in Table 2.

The case of a continuous injection of many small shards does not suffer from a requirement related to shard penetration, since RE seeds would be constantly depleted, such that the RE population would always remain far too small to vaporize shards (in addition, REs would not have the possibility to reach large energies). The linear density of pellet volume required to stop REs with this scheme (given in the first row of Table 1) does not depend on $\langle v_s \rangle$, while the injection rate is proportional to $1/\langle v_s \rangle$. If we assume $\langle v_s \rangle = 100$ m/s, we obtained required injection rates equivalent to 600 (resp. 90) 28 mm pellets/s for hydrogen (resp. neon or argon). Comparing these numbers to those in Table 2, it appears that for a strategy based on the injection of many small shards, a continuous injection requires a roughly twice smaller injection rate than a repeated injection, but required injection rates appear quite large in all cases. With a strategy based on a few large shards, the required injection rate are a bit smaller.

A delicate point is that shards take time to reach the center of the plasma. For example, at 100 m/s, they would take about 20 ms, which is much longer than the 5 ms allowable temporal gap found above. This suggests that one cannot afford to wait for the beginning of the CQ to start injections (unless magnetic stochasticity persists and deconfines REs for a long enough period, which is presently uncertain). A possible solution which would need to be explored is to rely on left-over shards from pre-TQ injections.

6. Effect of potentially ablated material on Current Quench timescale

The last critical aspect to consider in order to assess the feasibility of the proposed scheme is that if too much of the injected material is assimilated by the plasma, the CQ could become shorter than tolerable. Fig. 8 shows how the assimilation of a certain number of hydrogen (left), neon or argon (right) 28 mm pellets is expected to affect the CQ exponential timescale, $\tau_{\rm CQ}$. Red lines indicate the minimal and maximal tolerable values of $\tau_{\rm CQ}$. As in [5], we estimate the latter as $\tau_{\rm CQ} \simeq La^2/(2R_0\eta)$. We assume a plasma self-inductance $L = 5$ μH (corresponding to the above-mentioned 75 V.s, which accounts for the presence of the highly conductive vacuum vessel, divided by 15 MA), a minor radius $a = 2$ m and a major radius $R_0 = 6$ m. The resistivity is calculated as $\eta = 2.8\times10^{-8}\times Z_{\rm eff}/T_e^{3/2}$ with T_e in keV and $Z_{\rm eff} = (n_i+n_{\rm imp}Z_{\rm eff,imp})/(n_i+n_{\rm imp}\langle Z\rangle_{\rm imp})$. Here, $\langle Z\rangle_{\rm imp}$ is the averaged charge of the impurity, i.e. $\langle Z\rangle_{\rm imp} \equiv \sum_k Z_{\rm imp,k}n_{\rm imp,k}/n_{\rm imp}$, where the sum is over charge states of the impurity, and $Z_{\rm eff,imp}$ is the effective charge of the impurity, i.e. $Z_{\rm eff,imp} \equiv \sum_k n_{\rm imp,k}Z_k^2/(\langle Z\rangle_{\rm imp}n_{\rm imp})$. These quantities are functions of T_e obtained from ADAS data [13] assuming coronal equilibrium. The electron temperature is calculated from the power balance between Ohmic heating and radiative losses: $\eta j^2 = n_e n_{\rm imp} L_{\rm rad}$, where $n_e = n_{e0} + \langle Z\rangle_{\rm imp}n_{\rm imp}$, n_{e0} representing the electron density associated to the main ions. We assume $j = 1$ MA/m^2. The radiative cooling rate $L_{\rm rad}$ is a function of T_e calculated from ADAS data assuming coronal equilibrium.

It appears that for hydrogen pellets (left plot in Fig. 8), $\tau_{\rm CQ}$ is not strongly sensitive to the number of assimilated pellets. Typically, up to about 10 pellets could be assimilated while remaining within the tolerable $\tau_{\rm CQ}$ range. A caveat of our model is however that hydrogen radiation is not included, which could make a key difference and lead to plasma recombination for large amounts of assimilated material, as found in [9]. On the other hand, for neon or argon pellets, $\tau_{\rm CQ}$ is much more sensitive to the number of assimilated pellets. With the chosen parameters, the maximal tolerable amount of assimilated material is equivalent to about 1% (resp. 3%) of a 28 mm pellet for argon (resp. neon).

These tolerable amounts of assimilated material should be compared with predictions of the ablated quantities. However, ablation rate scalings, like provided in [15] for example, are not valid at typical CQ electron temperatures [16]. Future work should thus be devoted to modelling pellet ablation during the CQ.

However, even if ablation is sufficiently small, after travelling across the plasma, shards would hit the first wall and an important question is whether this could lead to material coming back towards the plasma, either in the form of gas, solid or liquid, and whether this could lead to more material assimilation.

7. Summary and outlook

Table 3 summarizes the injection rates required for shards to penetrate and stop REs (combining information from Tables 1 and 2). The unit used in this table is the

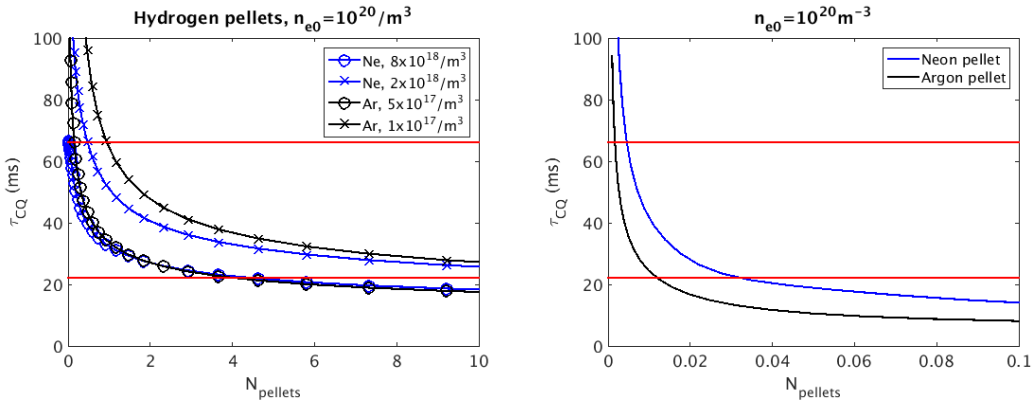


Figure 8. Current Quench exponential timescale as a function of the number of 28 mm pellets assimilated by the plasma, for hydrogen (left) and neon or argon pellets (right). The initial plasma is supposed to have an electron density of 10^{20} m^{-3} and, in the case of the hydrogen pellets, also neon or argon impurities whose densities are indicated in the legend.

	H	Ne	Ar
Many small shards, continuous	60	9	9
Many small shards, repeated	100	18	18
Single shard, repeated	30	6	6

Table 3. Required injection rate for shards to penetrate and stop REs, in terms of equivalent number of 28 mm pellets over 100 ms (see text for details).

equivalent number of 28 mm pellets that would need to be injected over a duration of 100 ms, i.e. roughly over the CQ duration. Note that the 'many small shards, repeated' case is probably the most relevant one for the present ITER DMS design since it is closest to what would be obtained with repeated SPI. Required pellet numbers are large, especially for hydrogen pellets for which they are beyond the capability of the present ITER DMS design (which cannot inject more than 24 pellets of 28 mm). On the other hand, for neon or argon, required numbers may be within reach, although technical aspects would need to be investigated.

Table 4 summarizes how many 28 mm pellets could be assimilated before the CQ becomes shorter than the lower bound set by electromagnetic loads (see Fig. 8). Note that another limit on material assimilation, which has not been addressed here, is set by the need to avoid 'doing more harm than good' in terms of RE generation and acceleration through increasing the electric field and adding partly ionized impurities to the background plasma. It can be seen that the assimilation limit due to electromagnetic loads is extremely small. For neon or argon in particular, there are more than two orders of magnitude difference between numbers in Tables 3 and 4, meaning that the assimilated fraction has to be smaller than 1%. The assimilation limit due to RE generation and acceleration is probably no more drastic than that, in an order of magnitude sense. The development of pellet ablation models in CQ plasmas, as well as experiments on SPI

	H	Ne	Ar
Max. # of assimilated 28 mm pellets for acceptable τ_{CQ}	5-10	0.03	0.01

Table 4. Maximum number of 28 mm pellets which could be assimilated before the CQ becomes too short.

during the CQ in present machines, would help assess whether such a low assimilation rate could be achieved.

Another aspect which needs to be looked into is the effect of the vertical plasma motion during the CQ. One should ensure that shards do not 'miss their target' as a result of this motion. An injection scheme ensuring a wide angular dispersion of the shards would be helfpul in this respect. Also, as noted above, the effect of magnetic islands should be investigated since they may result in some REs never interacting with shards.

Yet another question is what would happen to the plasma current. If shards are present in sufficient numbers to stop RE seeds, one may wonder if they might not also stop the current carried by the thermal electrons, which could have deleterious consequences e.g. in terms of electromagnetic loads. A direct blocking of the current on a macroscopic level can however be excluded because the large inductance of the system would imply breakdown in the shards before the current is suppressed [17]. Still, the presence of the shards might increase the global resistance and thereby decrease the CQ timescale. This question is left for future work.

It is important to stress that in the present study, we have considered only hydrogen, neon or argon as candidate materials in order to match the capabilities of the present ITER DMS design. However, thinking of a possible ITER DMS upgrade for the nuclear phase, other materials could be considered. A particularly interesting suggestion from Nick Eidietis would be to use small tungsten (W) pellets or grains coated with a low Z material. These would combine the large stopping power and vaporization energy of W with a weak effect on the CQ timescale from the ablation of the low Z material, and thus appear as an ideal solution. Of course, technical aspects would need to be assessed, like the formation and injection of such pellets or the effect of their impact on the wall after travelling across the plasma.

Finally, it would obviously be good to test the proposed scheme in present devices. This however requires a scenario that reliably produces very small, and at the same time measurable, RE populations during the CQ, which is a challenging task. This difficulty is related the large gap that separates ITER from present devices in terms of RE physics (especially during the nuclear phase, which is expected to combine small continuous seed generation with a very large avalanche gain), a gap that is hard to fill other than by theory and modelling.

8. Acknowledgements

The authors wish to thank P. Aleynikov, B. Breizman, M. Lehnen and B. Pégourié for useful discussions.

9. References

[1] M. Lehnen et al., J. Nucl. Mater. **463** 39–48 (2015)
[2] M. Lehnen et al., 27th IAEA Fusion Energy Conference, Gandinaghar, India, 2018
[3] B. Breizman et al., Nucl. Fusion **59** 083001 (2019)
[4] A. Boozer, Phys. Plasmas **22** 032504 (2015)
[5] J.R. Martín-Solís et al., Nucl. Fusion **57** 066025 (2017)
[6] C. Paz-Soldan et al., Nucl. Fusion **60** 056020 (2020)
[7] E. Nardon et al., Nucl. Fusion (2020), accepted for publication, https://doi.org/10.1088/1741-4326/abb749
[8] M.N. Rosenbluth and S.V. Putvinski, Nucl. Fusion **37** 1355 (1997)
[9] O. Vallhagen et al., J. Plasma Phys. **86** 475860401 (2020)
[10] A. Boozer, Plasma Phys. Control. Fusion **61** 024002 (2019)
[11] https://physics.nist.gov/PhysRefData/Star/Text/ESTAR.html
[12] M. Lehnen, private communication
[13] http://adas.ac.uk
[14] G Papp et al., Plasma Phys. Control. Fusion **53** 095004 (2011)
[15] V. Yu. Sergeev et al., Plasma Phys. Rep. **32** 363–377 (2006)
[16] B. Pégourié, private communication
[17] P. Aleynikov, private communication